

Coarse-to-Fine Active Segmentation of Interactable Parts in Real Scene Images

Ruiqi Wang¹, Akshay Gadi Patil¹, Fenggen Yu¹, Hao Zhang¹
¹Simon Fraser University



Figure 1: 2D segmentation results on *interactable* object parts in *real-world* indoor scene images. We show part segmentation masks obtained using similar methods, viz. OPD [15] and Mask2Former [7]. We also contrast the results of our proposed *pose-aware masked-attention* model, with and without Active Learning (AL) framework.

Abstract

We introduce the first active learning (AL) framework for high-accuracy instance segmentation of dynamic, interactable parts from RGB images of real indoor scenes. As with most human-in-the-loop approaches, the key criterion for success in AL is to minimize human effort while still attaining high performance. To this end, we employ a transformer-based segmentation network that utilizes a masked-attention mechanism. To enhance the network, tailoring to our task, we introduce a coarse-to-fine model which first uses object-aware masked attention and then a pose-aware one, leveraging a correlation between interactable parts and object poses and leading to improved handling of multiple articulated objects in an image. Our coarse-to-fine active segmentation module learns both 2D instance and 3D pose information using the transformer, which supervises the active segmentation and effectively reduces human effort. Our method achieves close to fully accurate (96% and higher) segmentation results on real images, with 77% time saving over manual effort, where the training data consists of only 16.6% annotated real photographs. At last, we con-

tribute a dataset of 2,550 real photographs with annotated interactable parts, demonstrating its superior quality and diversity over the current best alternative.

1. Introduction

Most objects we interact with in our daily lives have dynamic movable parts, where the part movements reflect how the objects function. Perceptually, acquiring a visual and actionable understanding of object functionality is a fundamental task. In recent years, motion perception and functional understanding of articulated objects have received increasing attention in computer vision, robotics, and VR/AR applications. Aside from per-pixel or per-point motion prediction, the segmentation of dynamic, *interactable* parts serves as the basis for many downstream tasks, including robot manipulation, action planning, and part-based 3D reconstruction.

In this paper, we tackle the problem of *instance* segmentation of interactable parts from RGB images of *real indoor scenes*. Most prior works on such segmentations [37, 17, 12] operate on point clouds, which are more expensive to capture than images while having lower resolution, noise, and

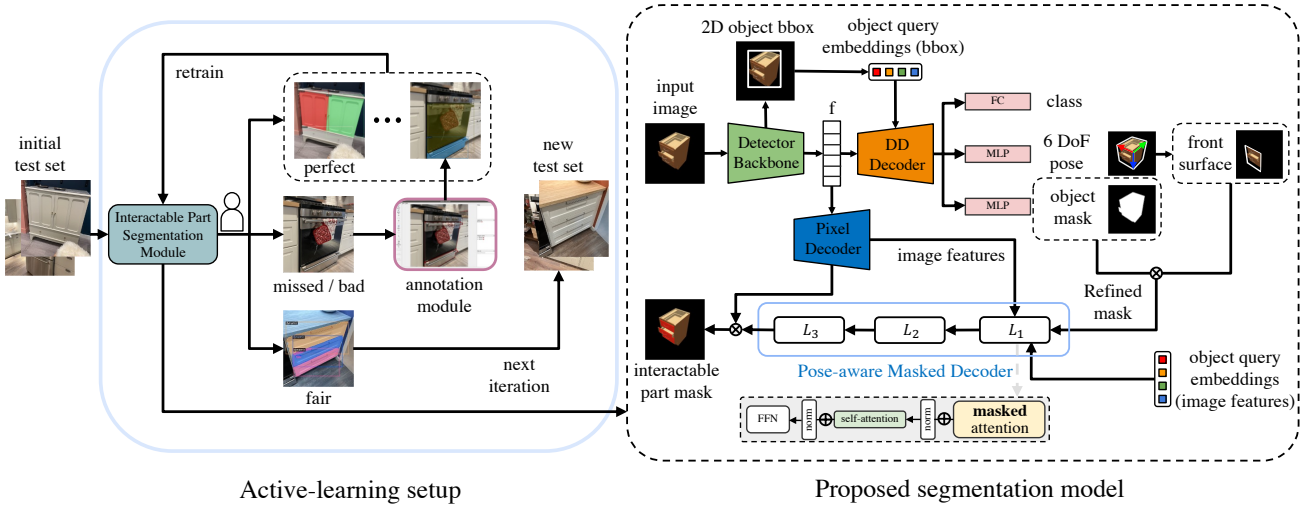


Figure 2: Overview of our coarse-to-fine active segmentation method for interactable parts in real scene images. Our active learning setup (shown on the left; see Section 3.4) makes use of a synthetically trained, transformer-based, coarse-to-fine 2D segmentation model (shown on the right; see Section 3.3) to obtain segmentation masks on unseen real images through iterative refinement via human-in-the-loop feedback.

outliers. To our knowledge, OPD [15], for “openable part detection”, represents the state-of-the-art in interactable part segmentation from images. However, their method was trained and evaluated only on *single* objects, not scenes, and there remains a large gap between synthetic and real test performances. The best reported accuracy on dynamic part segmentation from real images, by OPD, is only 45%.

Typical approaches to close the synthetic-to-real gap rely on domain adaptation using annotated real images, but the manual annotation process is highly tedious for instance segmentation. To this end, OPD[15] opted to manually annotate *mesh* models of real articulated 3D objects and then render them from many views to obtain OPDReal, a dataset of about 20K annotated images. However, there is an inevitable gap between projected images of *digitally reconstructed* 3D meshes and real photographs, with both reconstruction errors and re-projection errors further hindering image quality.

To address the above challenges, we present an *active learning* (AL) [3, 23, 38] approach to obtain high-accuracy instance segmentation of interactable parts from real scene images. AL is a semi-supervised learning paradigm, relying on human feedback to continually improve the performance of a neural segmentation model. As with most human-in-the-loop approaches, the key criterion for success in AL is to minimize human effort. To this end, we employ a transformer-based [9] segmentation network that utilizes a masked-attention mechanism [7]. To enhance the network for interactable part segmentation, we introduce a *coarse-to-fine* model which first uses an *object-aware* masked attention and then a *pose-aware* one, leveraging a correlation between dynamic parts and object poses and leading to improved

handling of multiple articulated objects in an image.

Our coarse-to-fine segmentation method learns both 2D instance and 3D pose information using the transformer network, which supervises the active segmentation and effectively reduces human effort. Unlike prior works on active segmentation [35, 27] which mainly focused on the efficiency of human annotation, our network learns the region-of-interests (ROI) from the pose-aware masked-attention decoder for better segmentation sampling in AL iterations.

In summary, our main contributions include:

- We introduce the first active learning framework for instance segmentation of dynamic/interactable parts from RGB images of real indoor scenes. Our method achieves close to fully accurate (96% and higher) segmentation results on real images, with 77% time saving over manual effort, where the training data consisting of only 16.6% annotated real photographs.
- We present a coarse-to-fine, object- and pose-aware masked-attention mechanism for active segmentation, leading to reduced human effort in AL and improved interactable part segmentation over state-of-the-art methods, including OPD [15] and Mask2Former [7].
- Our AL method has allowed us to annotate a dataset of 2,550 real photographs of articulated objects in indoor scenes. We show the superior quality and diversity of our new dataset over OPDReal, and the resulting improvements in segmentation accuracy.

2. Related Works

Articulated objects dataset. The last few years has seen the development of articulation datasets on 3D shapes. Of the many, ICON [11] build a dataset (unreleased) of 368 moving joints corresponding to various parts of 3D shapes from the ShapeNet dataset [6]. The Shape2Motion dataset [31] provides kinematic motions for 2,240 3D objects across 45 categories sourced from ShapeNet and 3D Warehouse [1]. The PartNet-Mobility dataset [34] consists of 2,374 3D objects across 47 categories from the PartNet dataset [20], providing motion annotations and part segmentation in 3D.

All these datasets are obtained via manual annotations and are *synthetic* in nature. Since sufficient training data is made available by these synthetic datasets, models trained on them can be used for fine-tuning on *real-world* 3D articulated object datasets with limited annotations.

A recent work, called OPD [15], provides a 2D image dataset of real-world articulated objects, OPDReal, obtained from RGB-D scans of indoor environments. The images in OPDReal come with 2D segmentation labels on all *openable* parts along with their motion parameters. However, due to the nature of annotation process, the 2D part segmentation masks obtained via 3D-to-2D projection do not completely cover all interactable parts in the image. Also, in OPDReal, objects are scanned from within a limited distance range. Practical scenarios and use cases are likely going to have large camera pose and distance variations.

To overcome these limitations, we contribute a 2D image dataset of articulated objects present in the real world (furniture stores, offices, homes), captured using iPhone12 Pro and 14. We then use our active-learning framework (see Figure 2 and Section 3) to learn a generalized 2D segmentation for interactable object parts.

Part segmentation in images. Early approaches [30, 29, 33] to 2D semantic part segmentation developed probabilistic models on human and animal images. While not addressing the 2D semantic part segmentation problem as such, [13, 19, 4, 16, 21] tackled the problem of estimating 3D articulations from human images, which requires an understanding of articulated regions in the input image.

Recently, with the availability of 3D part datasets [20, 34], there have been works that estimate 3D articulations from articulation images [2, 17, 39]. However, they learn a latent space of 3D articulation parameters and do not provide 2D segmentation masks for interactable parts. Our work aims at segmenting *interactable* parts of a 3D object from image input. To our knowledge, OPD [15] is the only work that can segment such object parts given an input image, and is built on the Mask RCNN architecture [10]. In our work, we employ the Mask2Former [7] architecture with task-specific modifications as described in Section 3.

Active learning for image segmentation. Active learning (AL) is a well-known technique for improving model

performance with limited labeled data. Prior works [24, 26, 5, 36, 25] have demonstrated different ways of using the most informative data to acquire labels with minimum cost for 2D segmentation task. There exist AL algorithms for 2D segmentation task [22, 32] that are specifically designed to reduce the domain gap by aligning two data distributions. We can not borrow such methods to reduce the domain gap between synthetic and real scene images of interactable objects because of large feature differences (our synthetic images contain no background, unlike real scene images).

More recently, [27, 35] employed AL to refine initial 2D segmentation mask through key point or region selection, requiring little human guidance. Due to potentially multiple interactable parts, such point/region selection are ambiguous for an interactable object. As such, we design an AL framework that reduces manual effort by focusing on: (a) using improved part segmentation model (see Section 3.3), and (b) simpler rules for modifying the test set for iterative model refinement (see Section 3.4).

3. Method

3.1. Terminology

For exposition clarity, we define some terms that are frequently used across much of this work.

Interactable objects – 3D shapes that contain moveable parts, such as a cabinet drawer, either in the rest state or in the articulated state, are said to be interactable objects.

Interactable parts – Moveable parts in interactable objects are called interactable parts. **Dynamic parts** – Dynamic parts and interactable parts are used interchangeably throughout.

Articulated objects – Interactable objects with articulations on their dynamic parts are termed as articulated objects.

3.2. Problem statement

Let D be a real-world image dataset of interactable objects. Given an RGB image $I \in D$ containing one or more interactable objects $\{o_j\}$ as input, our goal is to output a set of 2D segmentation masks, $\{m_i\}$, corresponding to all interactable parts for each object $o \in \{o_j\}$ present in I , where each mask m_i is represented by a 2D polygon.

We propose an active learning setup (for segmentation on unlabeled datasets) using a transformer model for continual mask refinement on unseen real images using a human-in-the-loop framework. Figure 2 provides an overview of our approach. It consists of two parts: (a) a pose-aware masked-attention network for 2D segmentation of interactable parts of $\{o_i\}$ in I , and (b) learning to generalize such segmentations using an active learning framework.

3.3. Pose-aware masked-attention network

Fig 2 (right) shows a detailed structure of our segmentation network, whose working can be broken down into five

Table 1: Dataset statistics for OPDReal and our datasets, over six object categories. Both datasets contain images with different object categories with multiple interactable parts. Our dataset is relatively more balanced in terms of sample distribution between different object categories, allowing models to generalize better on unseen images. We combine microwave and oven since objects in these two categories often appear together in real indoor scenes.

		Category				
OPDReal[15]	Objects	Storage	Fridge	Dishwasher	Micro.&Oven	Washer
	Images	231	12	3	12	3
	image %	27,394	1,321	186	823	159
Ours	Objects	91.67%	3.93%	0.62%	2.75%	0.53%
	Images	176	51	31	62	13
	image %	925	370	315	775	175
		36.27%	14.51%	12.35%	30.39%	6.8%

major steps as explained below.

Detector backbone. First, the input image I is passed through a *pre-trained* 2D object detection network, MaskRCNN[10], to obtain a 2D object bounding box $bbox^o$, and features maps, f for subsequent processing.

DD Decoder. We use the *pretrained* decoder from *Deformable DETR* transformer module proposed by Zhu et al.[40]. Inspired by [14], we replace the learned object query embedding with the normalization of centre coordinates (c_x, c_y) , width and height (w, h) from the detected 2D bounding box, so that the decoder can generate new object query embeddings which contain both local and global information extracted from the image, and the 2D bounding box can be used for 6DoF pose estimation.

Task-specific MLPs. Object queries from decoder are passed into three separate MLP heads, trained from scratch, for (a) object class prediction, (b) 6DoF object pose estimation and (c) binary object mask prediction. The class prediction head uses the cross-entropy loss, and the mask prediction head uses a pixel-wise cross-entropy loss.

The pose estimation head, predicting 6DoF object pose, outputs a rotation matrix \mathbf{R} , and translation matrix \mathbf{t} , against whom the loss function is formulated. Specifically, for \mathbf{t} , we use an L2 loss: $L_t = \|\mathbf{t} - \tilde{\mathbf{t}}\|_2$, and for \mathbf{R} , we use a geodesic loss as defined in [18]: $L_{rot} = \arccos \frac{1}{2} \left(Tr \left(\mathbf{R} \tilde{\mathbf{R}}^T \right) - 1 \right)$, where $\tilde{\mathbf{t}}$, $\tilde{\mathbf{R}}$ are predictions. The loss for pose estimation head is: $L = \lambda_t L_t + \lambda_{rot} L_{rot}$, where λ_t and λ_{rot} are the weighting parameters, set to 2 and 1 respectively.

Using $bbox^o$ and the estimated 6DoF object pose, we can obtain the corresponding 3D *oriented* bounding box OBB^o , which tightly fit the $bbox^o$. From among the eight vertices in OBB^o , we select vertices of the face with positive x coordinates as the representative 2D box for object front, and use it to crop the input image. This cropped image may contain pixels that do not actually belong to the object of interest. We filter out such pixels by multiplying it with the 2D binary object mask, resulting in a refined binary object

mask, m_{rfnd}^o .

Pixel decoder We borrow the the *pretrained* pixel decoder from MaskFormer [8] which takes f as input, and upsamples the features to generate embeddings f_{pd} .

Masked-attention decoder. To finally output segmentation masks corresponding to the interactable parts in I , we make use of masked-attention decoders from Mask2Former [7]. The structure of each layer L_i is shown right below L_1 in Figure 2. L_1 takes as input f_{pd} and the refined mask, m_{rfnd}^o and outputs a binary mask which is fed to the next layer. The binary mask at the output of L_3 is multiplied with f_{pd} resulting in part segmentation in the RGB space. The loss here is the pixel-wise cross entropy loss. We call it as our *pose-aware masked-attention decoder*.

All these modules are *jointly* trained in an *end-to-end* fashion for synthetic image datasets (see Section 4). When finetuning on real images where part annotations are made available, weights for all the modules, except the MLPs, are updated as GT pose and object masks are not collected for these images, which are required to train these MLPs.

3.4. Active learning for 2D part segmentation

In the active learning setup, we first consider a mini dataset, $E \in D$ of m images, and use it to improve our segmentation model with a human-in-the-loop framework. We call this mini dataset E the enhancement set as it iteratively helps enhance the segmentation masks at the output of our model. Next, we consider a really small training set, $T_s \in D$ (s.t $T_s \cap E$ is a nullset), of r images, and fine-tune our model M_s on this very small training set. As expected, M_s fine-tuned on T_s does not generalize well to images in E . This is where the active learning framework kicks in. In our implementation, $m = 500$, and $r = 50$.

We input images from E to the fine-tuned model M_s , which outputs segmentation masks for interactable parts in the input image. three scenarios exist: (1) If the output mask is deemed to be perfect (i.e., covers all interactable parts without any holes), as determined by humans, we move

such an example from E to T_s . So, $|E|$ and $|T_s|$ are now decreased and increased by 1, respectively; (2) If the output mask is imperfect (i.e., holes exist in predicted masks and/or not all interactable parts are segmented), we keep that sample as-is in E . And, (3) if the output is deemed to be bad (i.e., no interactable part is segmented), we obtain manual annotation for segmentation masks on all interactable parts from humans in the loop.

Once annotated, the examples are now “perfect” and moved from E to T_s . This process continues iteratively until all the examples in E are moved to T_s , resulting in $|E|$ being zero; see Table 6. This framework allows M_s to continually see new and good labeled training data on previously unseen images, helping it to learn better. We will show more details of human verification and annotation process in our supplementary material.

4. Datasets and Pre-training

Datasets. We use two kinds of real image datasets in our experiments: (1) images from the OPDReal dataset [15], and (2) images from our dataset. Our dataset images are obtained from the real world by taking photographs of interactable objects in indoor scenes from furniture stores, offices, and homes, captured using iPhone12 Pro and iPhone14. On average, each interactable object is photographed from five distinct viewpoints with varying camera poses and distances from the objects. Also, a captured image can contain more than one object with interactable parts. As such, our dataset is quite diverse compared to OPDReal, where objects are scanned from within a limited distance range.

For both datasets, we consider six object categories – Storage, Fridge, Dishwasher, Microwave, Washer, and Oven. The data distribution of 3D objects per category and their 2D images are shown in Table 1. In total, our dataset contains 2,550 images and OPDReal contains ~ 23 K images. Unlike OPDReal where part segmentation masks are manually annotated on a 3D mesh and then projected back to the image space, for our dataset, we obtain manual annotations (i.e., the ground truth) for 2D segmentation masks directly on the captured images. Note that such manual annotations are used only to evaluate our active learning framework.

From Table 1, we observe that the majority of data samples in OPDReal belong to the Storage category (91.67%), with the rest distributed among the remaining categories. The difference in distribution between the largest and the second largest category is 87.74%, and between the largest and smallest categories is 91.14%. With such data skewness towards one category, models trained on OPDReal will likely overfit to the dominant category. Our dataset, on the other hand, contains smaller variations in data distributions across the six object categories, where the difference in data distribution between the largest and second largest categories is 5.88%, and between the largest

and smallest categories is 29.47%.

Pre-training. We begin our experiments by rendering synthetic models from the PartNet-Mobility dataset [34] in various articulation states since this enables us to obtain sufficient annotations to train 2D segmentation networks and thus enable transfer learning applications. Our synthetic dataset contains around 32K articulation images, with equal data samples for each object category. We use a 90%-10% train-test split to train on this synthetic dataset, and use this trained model for fine-tuning on real images. To this end, we use all data samples from both datasets, OPDReal and ours, with 80%-20% train-test split.

We implement our network in PyTorch on a Nvidia RTX 2080 Ti GPU. All images are resized to 256×256 for training. During pre-training on the PartNet-Mobility dataset, we use the Adam optimizer with a learning rate (lr) of 2.5e-4, and train for 2K epochs. When fine-tuning on real images, we use the same lr and run for 4.5K epochs.

5. Results and Evaluation

We evaluate our pose and mask-aware interactable part segmentation model on real scene images (both ours and OPDReal) by comparing its segmentation results against two competing methods. Through ablation studies, we provide insights into the need for pose-aware and mask-aware components present in our network. Finally, we compare the segmentation results on *our* real scene images, with and without the active learning framework.

5.1. Competing Methods

OPD [15]. As one of the first (and only) works for detecting interactable object parts for in RGB images, we use OPD as one of our comparisons. In our experiments, we select OPDRCNN-C for comparison.

Mask2Former [7]. As an advanced, transformer-based extension of Mask RCNN architecture for generalized object detection and segmentation in 2D images, we compare against the Mask2Former architecture by employing it to detect all interactable object parts in input images.

5.2. Model ablations

The performance of our method is driven, in parts, by two specially designed prediction branches that individually output camera pose and object mask. We perform evaluations by ablating these two modules in our network architecture.

Ours w/o pose prediction branch. Keeping all other modules, we remove that MLP branch in Figure 2 which predicts 6 DoF camera pose for a given input image.

Table 2: Quantitative comparison against competing 2D part segmentation methods on test set images from OPDReal and our dataset. This is not using active learning.

segm mAP / bbox mAP (\uparrow)			
	OPD-C[15]	M2F[7]	Ours
OPDReal	37.380 / 44.663	39.380 / -	48.168 / 54.393
Ours	85.533 / 85.994	93.118 / -	96.592 / 96.699

Ours w/o object mask prediction branch. Here, we only remove that MLP branch in Figure 2 which predicts a binary object mask for the interactable objects (not parts) in the input image.

5.3. Evaluation Metrics

Mean Average Precision (mAP). Following OPD [15], we report mAP@IoU=0.5 scores for both 2D bounding box detection and 2D segmentation tasks. For brevity, in the rest of the section, we use mAP to denote mAP@IoU=0.5.

Annotation time. In the active learning setup, the key components that determine the need and efficiency of human-in-the-loop framework are the number of manual annotations, the annotation time (measured in hours), and segmentation accuracy (mAP@IoU=0.5).

Figure 3 and 4 show visual results on different models for test images from OPDReal and our dataset, respectively.

5.4. Quantitative results w/o active learning

We start off by comparing the performance of our model with competing methods without any active learning framework. As explained in Section 4, all these models are pre-trained on synthetic renderings, which are then fine-tuned using images from the two OPDReal and our dataset. Our primary interest in the 2D part segmentation performance. As such, we report the segmentation mAP(@IoU=0.5) on both, the OPDReal dataset and our dataset. For completeness of evaluation, we also report the mAP scores for 2D bounding box corresponding to interactable parts. These results are tabulated in Table 2.

We observe that our model significantly outperforms competing methods on both datasets. This proves the efficacy of our model over competing methods. It is interesting to note the big jump in performance for *all* the models when testing using models fine-tuned on our dataset, compared to their respective performance when fine-tuned on the OPDReal dataset. This is mainly due to data skewness towards the Storage category in OPDReal (makes for 91.67% of the total samples), leading to a lack of generalizability on images with other object categories. Since our dataset is relatively balanced across different categories (except for the Washer), we observe that all three models perform much better than



Figure 3: Qualitative results on OPDreal test set. “Miss” represents the absence of part segmentation with $\geq 75\%$ confidence. Both OPDRCNN-C and mask2former fail to detect some/all dynamic parts for categories with fewer samples (ex. Washer and Dishwasher). Our method outperforms the two – on part edges (first and second row), for noisy GT (third row), and on multiple objects (last row).

Table 3: Ablation study on our key components (no AL).

Row ID	Object Mask	Pose	segm mAP (\uparrow)
0	-	-	93.118
1	✓	-	94.542
2	-	✓	96.016
3	✓	✓	96.592

OPDReal counterparts, with our model achieving the best results again. These results validate the richness of our dataset over OPDReal for dynamic part segmentation tasks.

5.5. Ablation studies w/o active learning

We perform ablations on our network architecture to better understand the need for pose estimation MLP and the object mask prediction MLP at the output of the transformer decoder (shown in the orange-colored box on the right side of Figure 2). The segmentation performance is tabulated in Table 3. Essentially, when both the pose estimation module and the mask predictor module are removed (row 1), our network reduces to the architecture of Mask2Former [7]. Also, the pose estimation module seems to play more of a role than the object mask predictor module in achieving better part segmentation, with a positive net difference of 1.5% in mAP score, see row 3 and row 2 in Table 3, respectively.

This is because estimating 6-DoF pose enables us to obtain regions of interactable parts for objects in the image,

Table 4: Quantitative comparison against competing methods without AL and our AL framework. (50train/500test)

	AL	segm / bbox mAP (\uparrow)	Time (hr)
OPDRCNN-C	-	62.190 / 63.630	-
Mask2Former	-	75.626 / -	-
Ours	-	88.088 / 88.242	-
Ours	✓	97.780 / 97.780	1.675

whereas a coarse object binary mask provides information about the object as a whole. When both modules are present (row 4), the network achieves the best performance since they provide a coarse-to-fine refinement over their individual contributions. This is nothing but our setting.

5.6. Quantitative results with active learning

The learning framework and data modifications per iteration in the active learning (AL) setup are described in Section 3.4. In Table 4, we present the mAP scores for different models, and contrast them with the active learning setup on our model, on the same train-test set of 50-500 real-world images. Naturally, all models without AL framework overfit on the 50-image training set, with the performance of the *best* model being $\sim 10\%$ lower than our AL framework.

We also compare annotation times required for labeling all images in our enhancement set (see Section 3.4) purely based on segmentation results output from OPD and Mask2Former. That is, no active learning is considered here. Table 5 presents these results and compares them against our AL framework. We clearly see that the number of images as well as interactable parts that need manual annotation to segment all interactable parts is greater for OPD, followed by Mask2Former. However, this number drops drastically when our AL model is considered. As such, our AL model consumes the least time to get 2D segmentation masks.

Finally, we also show the AL process for all four iterations in Table 6. The important thing to read in this table are the last three columns that represent the number of images/part with “perfect” segmentations, and the amount of time taken to fix them, respectively (see Section 3.4 for interpretation of “perfect” and “bad”). We observe that as the iterations progress, the amount of annotation time decreases, which can be attributed to the model’s generalization ability with more labeled training data.

5.7. Ablation studies with active learning

In Table 7, we show timing comparisons for annotating enhancement set images (refer to Section 3.4 for terminology) using different versions of our model. We again observe that the pose estimation module (Row ID 2) provides better segmentation masks on unseen images compared to the object mask prediction module (Row ID 1), resulting in less

Table 5: Comparison of different methods in *manually* annotating segmentation masks for images in our enhancement set.

Method	#Images/Parts.	Time (hr) \downarrow
OPDRCNN-C	483 / 1640	7.25
Mask2Former	324 / 1102	5.01
ours (AL)	83 / 239	1.675

Table 6: Different data and efficiency statistics over each iteration of the active learning process on enhancement set.

Iter.	Train	Test	Perfect	Bad	Time (hr)
0	50	500	-	-	-
1	340	210	260	30 / 97	0.82
2	445	105	82	23 / 53	0.39
3	550	-	75	30 / 89	0.46

Table 7: Ablation study on key modules of our method with active learning on our enhancement set.

Row ID	Object Mask	Pose	Time (hr) \downarrow
0	-	-	3.882
1	✓	-	2.302
2	-	✓	1.854
3	✓	✓	1.675

human intervention for rectifying the masks, as recorded by the annotation time in the last column. Our proposed model (Row ID 3) requires minimum time effort from humans, validating, yet again, our network design choices.

6. Conclusion

We advocate active learning as a general and effective means to obtain high-accuracy instance segmentations. It may be the most viable option to achieve close-to-error-free performance on arbitrary test sets. If properly designed, AL can significantly reduce human annotation effort for dataset preparation. In this work, we realized both goals for the specific task of instance segmentation of interactable parts from real scene images containing articulated objects.

Our contribution also includes a high-quality and diverse dataset of annotated real photographs, which we will continue to scale up to serve the vision community. We would also like to endow the annotated parts with motion parameters. On the technical side, there is much room to improve on speeding up the correction of erroneous segmentations during AL. Additional priors beyond object poses may also be explored to facilitate dynamic part segmentation. At last, we would like to extend our AL framework to other motion- or functionality-aware vision and annotation tasks.

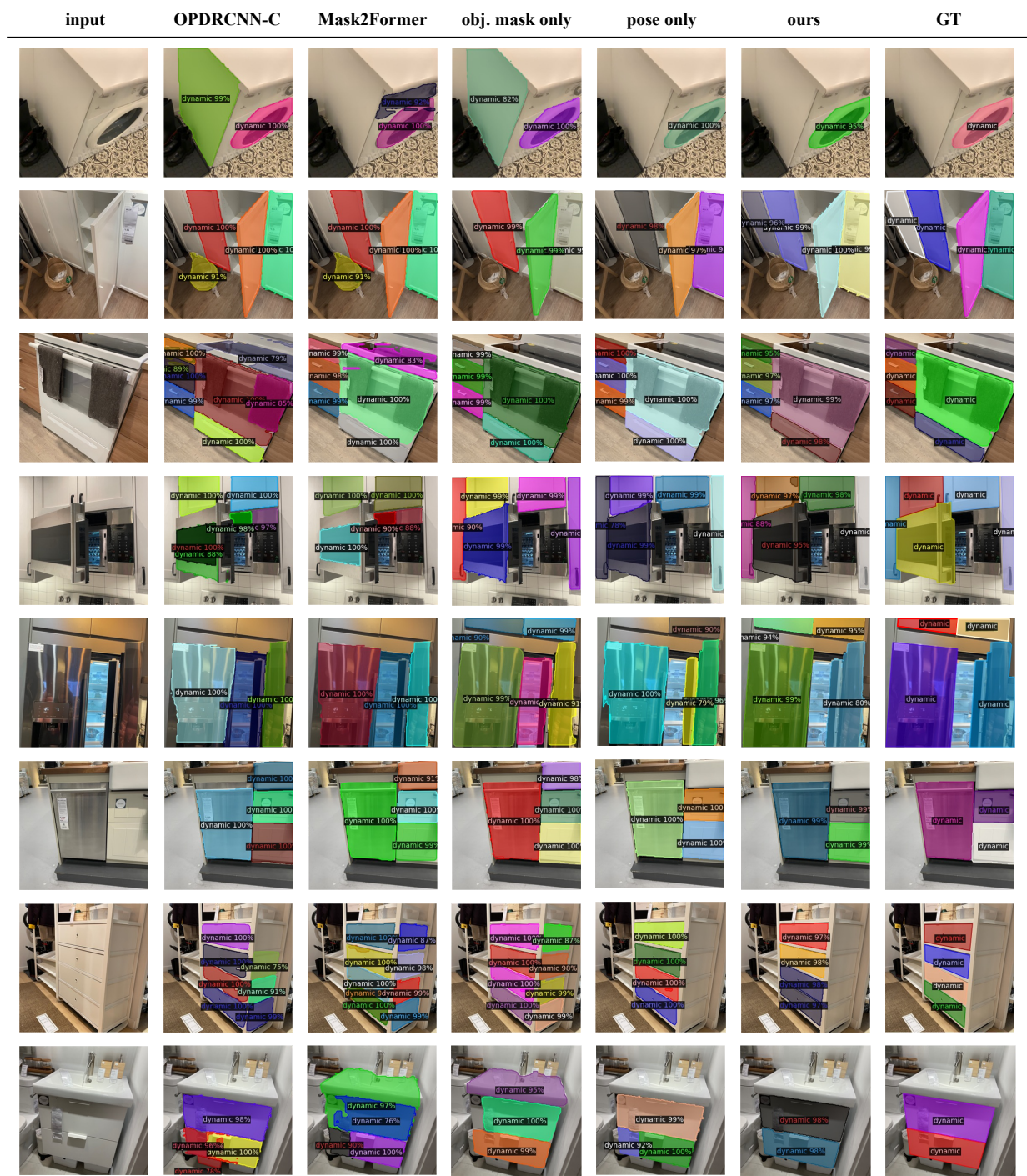


Figure 4: Qualitative results for test-set images from our dataset. Left to right – Prediction results using OPDRCNN-C [15], Mask2Former[7], our method using only the object mask prediction branch (i.e., without the pose estimation branch), our method using only the pose estimation branch (i.e., without the object mask prediction branch), our method (i.e., with both prediction branches), and the ground truth (GT). We show results on different object categories, and observe that our method outputs better segmentation masks over interactable parts, even when multiple objects exist in the input image. Our results also show that the existence of object mask predictor and pose estimator modules can effectively reduce segmentation errors from unwanted objects (second row) and object side surfaces(first, fifth and last rows). More results in the supplementary material.

References

[1] Trimble Inc. 3D Warehouse. <https://3dwarehouse.sketchup.com/>, 2023. Accessed: 2023-3-4. 3

[2] Ben AbbateMatteo, Stefanie Tellex, and George Konidaris. Learning to generalize kinematic models to novel objects. In *Proceedings of the 3rd Conference on Robot Learning*, 2019. 3

[3] Charu C. Aggarwal, Xiangnan Kong, Quanquan Gu, Jiawei Han, and Philip S. Yu. Active learning: A survey. In *Data Classification: Algorithms and Applications*, pages 571–597. 2

[4] Luca Ballan, Aparna Taneja, Jürgen Gall, Luc Van Gool, and Marc Pollefeys. Motion capture of hands in action using discriminative salient points. In *Computer Vision–ECCV 2012: 12th European Conference on Computer Vision, Florence, Italy, October 7–13, 2012, Proceedings, Part VI 12*, pages 640–653. Springer, 2012. 3

[5] Arantxa Casanova, Pedro O Pinheiro, Negar Rostamzadeh, and Christopher J Pal. Reinforced active learning for image segmentation. In *International Conference on Learning Representations*, 2020. 3

[6] Angel X Chang, Thomas Funkhouser, Leonidas Guibas, Pat Hanrahan, Qixing Huang, Zimo Li, Silvio Savarese, Manolis Savva, Shuran Song, Hao Su, et al. Shapenet: An information-rich 3d model repository. *arXiv preprint arXiv:1512.03012*, 2015. 3

[7] Bowen Cheng, Ishan Misra, Alexander G Schwing, Alexander Kirillov, and Rohit Girdhar. Masked-attention mask transformer for universal image segmentation. In *Proceedings of the IEEE/CVF Conference on Computer Vision and Pattern Recognition*, pages 1290–1299, 2022. 1, 2, 3, 4, 5, 6, 8, 11

[8] Bowen Cheng, Alex Schwing, and Alexander Kirillov. Per-pixel classification is not all you need for semantic segmentation. *Advances in Neural Information Processing Systems*, 34:17864–17875, 2021. 4

[9] Alexey Dosovitskiy, Lucas Beyer, Alexander Kolesnikov, Dirk Weissenborn, Xiaohua Zhai, Thomas Unterthiner, Mostafa Dehghani, Matthias Minderer, Georg Heigold, Sylvain Gelly, et al. An image is worth 16x16 words: Transformers for image recognition at scale. *arXiv preprint arXiv:2010.11929*, 2020. 2

[10] Kaiming He, Georgia Gkioxari, Piotr Dollár, and Ross Girshick. Mask r-cnn. In *Proceedings of the IEEE international conference on computer vision*, pages 2961–2969, 2017. 3, 4

[11] Ruizhen Hu, Wenchao Li, Oliver Van Kaick, Ariel Shamir, Hao Zhang, and Hui Huang. Learning to predict part mobility from a single static snapshot. *ACM Transactions on Graphics (TOG)*, 36(6):1–13, 2017. 3

[12] Jiahui Huang, He Wang, Tolga Birdal, Minhyuk Sung, Federica Arrigoni, Shi-Min Hu, and Leonidas J Guibas. Multi-bodysync: Multi-body segmentation and motion estimation via 3d scan synchronization. In *Proceedings of the IEEE/CVF Conference on Computer Vision and Pattern Recognition*, pages 7108–7118, 2021. 1

[13] Zeng Huang, Yuanlu Xu, Christoph Lassner, Hao Li, and Tony Tung. Arch: Animatable reconstruction of clothed humans. In *Proceedings of the IEEE/CVF Conference on Computer Vision and Pattern Recognition*, pages 3093–3102, 2020. 3

[14] Thomas Jantos, Mohamed Hamdad, Wolfgang Granig, Stephan Weiss, and Jan Steinbrener. PoET: Pose Estimation Transformer for Single-View, Multi-Object 6D Pose Estimation. In *6th Annual Conference on Robot Learning (CoRL 2022)*. 4

[15] Hanxiao Jiang, Yongsen Mao, Manolis Savva, and Angel X Chang. Opd: Single-view 3d openable part detection. In *Computer Vision–ECCV 2022: 17th European Conference, Tel Aviv, Israel, October 23–27, 2022, Proceedings, Part XXXIX*, pages 410–426. Springer, 2022. 1, 2, 3, 4, 5, 6, 8, 11, 12

[16] Angjoo Kanazawa, Michael J Black, David W Jacobs, and Jitendra Malik. End-to-end recovery of human shape and pose. In *Proceedings of the IEEE conference on computer vision and pattern recognition*, pages 7122–7131, 2018. 3

[17] Xiaolong Li, He Wang, Li Yi, Leonidas J Guibas, A Lynn Abbott, and Shuran Song. Category-level articulated object pose estimation. In *Proceedings of the IEEE/CVF Conference on Computer Vision and Pattern Recognition*, pages 3706–3715, 2020. 1, 3

[18] Siddharth Mahendran, Haider Ali, and René Vidal. 3d pose regression using convolutional neural networks. In *Proceedings of the IEEE International Conference on Computer Vision Workshops*, pages 2174–2182, 2017. 4

[19] Dushyant Mehta, Srinath Sridhar, Oleksandr Sotnychenko, Helge Rhodin, Mohammad Shafiei, Hans-Peter Seidel, Weipeng Xu, Dan Casas, and Christian Theobalt. Vnect: Real-time 3d human pose estimation with a single rgb camera. *AcM transactions on graphics (tog)*, 36(4):1–14, 2017. 3

[20] Kaichun Mo, Shilin Zhu, Angel X. Chang, Li Yi, Subarna Tripathi, Leonidas J. Guibas, and Hao Su. PartNet: A large-scale benchmark for fine-grained and hierarchical part-level 3D object understanding. In *The IEEE Conference on Computer Vision and Pattern Recognition (CVPR)*, June 2019. 3

[21] Franziska Mueller, Florian Bernard, Oleksandr Sotnychenko, Dushyant Mehta, Srinath Sridhar, Dan Casas, and Christian Theobalt. GANerated hands for real-time 3d hand tracking from monocular rgb. In *Proceedings of the IEEE conference on computer vision and pattern recognition*, pages 49–59, 2018. 3

[22] Munan Ning, Donghuan Lu, Dong Wei, Cheng Bian, Chenglang Yuan, Shuang Yu, Kai Ma, and Yefeng Zheng. Multi-anchor active domain adaptation for semantic segmentation. In *Proceedings of the IEEE/CVF International Conference on Computer Vision*, pages 9112–9122, 2021. 3

[23] Pengzhen Ren, Yun Xiao, Xiaojun Chang, Po-Yao Huang, Zhihui Li, Brij B. Gupta, Xiaojiang Chen, and Xin Wang. A survey of deep active learning, 2020. 2

[24] Ozan Sener and Silvio Savarese. Active learning for convolutional neural networks: A core-set approach. In *International Conference on Learning Representations*, 2018. 3

[25] Gyungin Shin, Weidi Xie, and Samuel Albanie. All you need are a few pixels: Semantic segmentation with pixelpick. In *Proceedings of the IEEE/CVF International Conference on Computer Vision (ICCV) Workshops*, pages 1687–1697, October 2021. 3

[26] Samarth Sinha, Sayna Ebrahimi, and Trevor Darrell. Variational adversarial active learning. In *Proceedings of the IEEE/CVF International Conference on Computer Vision (ICCV)*, October 2019. 3

[27] Chufeng Tang, Lingxi Xie, Gang Zhang, Xiaopeng Zhang, Qi Tian, and Xiaolin Hu. Active pointly-supervised instance segmentation. In *Computer Vision–ECCV 2022: 17th European Conference, Tel Aviv, Israel, October 23–27, 2022, Proceedings, Part XXVIII*, pages 606–623. Springer, 2022. 2, 3

[28] Kentaro Wada. labelme: Image polygonal annotation with python. <https://github.com/wkentaro/labelme>, 2018. 12

[29] Jianyu Wang and Alan L Yuille. Semantic part segmentation using compositional model combining shape and appearance. In *Proceedings of the IEEE conference on computer vision and pattern recognition*, pages 1788–1797, 2015. 3

[30] Peng Wang, Xiaohui Shen, Zhe Lin, Scott Cohen, Brian Price, and Alan L Yuille. Joint object and part segmentation using deep learned potentials. In *Proceedings of the IEEE International Conference on Computer Vision*, pages 1573–1581, 2015. 3

[31] Xiaogang Wang, Bin Zhou, Yahao Shi, Xiaowu Chen, Qinpeng Zhao, and Kai Xu. Shape2motion: Joint analysis of motion parts and attributes from 3d shapes. In *Proceedings of the IEEE/CVF Conference on Computer Vision and Pattern Recognition*, pages 8876–8884, 2019. 3

[32] Tsung-Han Wu, Yi-Syuan Liou, Shao-Ji Yuan, Hsin-Ying Lee, Tung-I Chen, Kuan-Chih Huang, and Winston H Hsu. D2ada: Dynamic density-aware active domain adaptation for semantic segmentation. In *Computer Vision–ECCV 2022: 17th European Conference, Tel Aviv, Israel, October 23–27, 2022, Proceedings, Part XXIX*, pages 449–467. Springer, 2022. 3

[33] Fangting Xia, Peng Wang, Xianjie Chen, and Alan L Yuille. Joint multi-person pose estimation and semantic part segmentation. In *Proceedings of the IEEE conference on computer vision and pattern recognition*, pages 6769–6778, 2017. 3

[34] Fanbo Xiang, Yuzhe Qin, Kaichun Mo, Yikuan Xia, Hao Zhu, Fangchen Liu, Minghua Liu, Hanxiao Jiang, Yifu Yuan, He Wang, Li Yi, Angel X. Chang, Leonidas J. Guibas, and Hao Su. SAPIEN: A simulated part-based interactive environment. In *The IEEE Conference on Computer Vision and Pattern Recognition (CVPR)*, June 2020. 3, 5

[35] Binhui Xie, Longhui Yuan, Shuang Li, Chi Harold Liu, and Xinjing Cheng. Towards fewer annotations: Active learning via region impurity and prediction uncertainty for domain adaptive semantic segmentation. In *Proceedings of the IEEE/CVF Conference on Computer Vision and Pattern Recognition*, pages 8068–8078, 2022. 2, 3

[36] Shuai Xie, Zunlei Feng, Ying Chen, Songtao Sun, Chao Ma, and Mingli Song. Deal: Difficulty-aware active learning for semantic segmentation. In *Proceedings of the Asian Conference on Computer Vision (ACCV)*, November 2020. 3

[37] Zihao Yan, Ruizhen Hu, Xingguang Yan, Luanmin Chen, Oliver Van Kaick, Hao Zhang, and Hui Huang. Rpm-net: recurrent prediction of motion and parts from point cloud. *arXiv preprint arXiv:2006.14865*, 2020. 1

[38] Xueying Zhan, Qingzhong Wang, Kuan-hao Huang, Haoyi Xiong, Dejing Dou, and Antoni B. Chan. A comparative survey of deep active learning, 2022. 2

[39] Ge Zhang, Or Litany, Srinath Sridhar, and Leonidas Guibas. Strobenet: Category-level multiview reconstruction of articulated objects. *arXiv preprint arXiv:2105.08016*, 2021. 3

[40] Xizhou Zhu, Weijie Su, Lewei Lu, Bin Li, Xiaogang Wang, and Jifeng Dai. Deformable detr: Deformable transformers for end-to-end object detection. *arXiv preprint arXiv:2010.04159*, 2020. 4

Supplementary Material

We present additional results, both qualitative and quantitative, here in the supplementary material. We begin by showcasing differences in examples of real scene images from our dataset and compare them with the kind of real images from OPDReal [15] dataset (Section A). We then present additional qualitative and quantitative results for 2D segmentation masks on interactable parts of objects in real scene images (Section B), without any active learning (AL) setup. We conclude the supplementary material by providing more results on different models (OPD [15], Mask2Former [7], and ours) using the human-in-the-loop framework (Section C). We also attach a video in the supplementary package that demonstrates human feedback in the active learning setup.

A. Dataset Visualization

We show more visualizations of raw images as well as annotated segmentation masks for interactable object parts in both, OPDReal dataset and ours, in Fig 5 and 6, respectively.

We show examples in our dataset from different categories. We can observe from the visualizations that the segmentation masks in OPDReal are not correctly annotated, with clear misalignments at part boundaries; see Fig 5(a) row 1, 4 right and, 6; Fig 6(a) row 1 left, 4 right, 5 left). In addition, due to reconstruction errors in OPDReal, some images are poorly labeled with noisy annotations, especially on objects with reflective surfaces such as the ones shown in Fig 5(a) row 2 right, 10 left and Fig 6(a) row 2, 9 right. As mentioned in our paper, OPD model is only used on images that contain a single instance of interactable objects. So, although there are multiple articulated objects in an image, only one of them will be annotated as seen in Fig 5(a), row 7 left, 9 left; Fig 6(a), row 9 right, 10 right.

Apart from annotation quality, the OPDReal dataset is not guaranteed to have high-resolution images. Image data of OPDReal are captured through frames from videos, which are used for 3D reconstruction. Therefore, some images have motion blur as seen in Fig 5(a), row 7 right, row 8 left and; Fig 6(a) row 3 right, row 4 right, row 8 right), and are not captured from clean viewing angles, which makes the target part look obscure, as seen in Fig 5(a) row 2 left, row 3 left, row 4 left, row 5, row 7 right, row 8, row 9 right, row 10 right.

In our dataset, images are directly labeled in 2D. Hence, we have a rich image dataset quality and contain clear annotations of interactable parts for more than one object present in an image. We present visualizations of individual categories of objects in our dataset along with their segmentation masks, see Fig 5(b-c), and Fig 6(b-d).

B. More Visualizations w/o Active Learning

We show additional qualitative results of different methods on our test set in Fig 7, 8, and on OPDReal dataset in Fig 9, 10, without the active learning setup.

On both datasets, our model outperforms the other two methods. It is worth noting that the segmentation results on OPDReal dataset using our method are superior to the so-called ground truth, as could be seen in the refinements of segmentation masks in Fig 9, Fig 10. Our methods is also able to detect multiple interactable objects in the same image.

C. More Results with Active Learning

In the active learning (AL) setup where we use feedback from humans in the loop, one of the major tasks is to judge the quality of annotations output from the base model used in the setup. To do this, we categorize the outputs into three types, and based on this categorization, the images are then moved to respective parts of the pipeline as described below.

Perfect If the model prediction precisely segments all interactable parts of objects in the image, the prediction will be considered as perfect, and it will be automatically moved to the training set from the enhancement set. Note that not all objects will be segmented in our task - if the object is too small or only partly shown in the image, it will be ignored as they are not meaningful in future downstream tasks.

Fair If the model prediction outputs partial segmentation masks with some minor mistakes (such as holes in the mask, noisy boundary, or wrong prediction on the background/side face of the object), then such a prediction will be considered as fair, and it will remain in the enhancement set for the next iteration.

Bad If the model fails to segment interactable object parts, or incorrectly segments a non-interactable part (such as combining two interactable parts together, wrong segmentation boundary, or missing too many interactable parts), then the prediction will be considered as bad. These bad predictions will be manually annotated and merged to the training set. Note that at every iteration, a bad prediction will be automatically selected from a completely missed prediction (no prediction with more than 75% confidence). Humans only needs to review the remaining predictions.

Fig 11 shows a comparison of perfect, fair, and bad predictions based on our model employed in the AL setup.

C.1. Quantitative and Qualitative Results

In Tables 8, 9, we present additional qualitative results in the active learning context when Mask2Former [7] and OPD

[15] are employed as the base models. Similar to the main paper where we present a table enumerating different data stats over each iteration of the active learning process, the above two tables are similar in spirit. These results are over the enhancement set of 500 images.

We observe that OPD and Mask2Former take 7 iterations in the AL setup, whereas our model (see the main paper, Table 6) takes only 4 iterations. Among the two competing methods, Mask2Former consumes less time over OPD, indicating that the predictions from Mask2Former are superior to OPD.

Finally, in Table 10, we also show the iteration process for our model in the AL setup on a new enhancement set of 2K images, which were previously used as the true test set. In Figure 11, we present visualizations of segmentation masks on the 2K enhancement set using our model.

C.2. User Study

We conduct an in-lab user study to (i) obtain timing in reviewing the model predictions after each iteration, and (ii) obtain timing for manually annotating the bad predictions. We selected 7 users with basic computer operating skills. We provided them with the same tools and instructions as used for the justification of prediction results and labeling of interactable parts in the AL process. They were tasked to distinguish perfect, fair and bad predictions from visualization results, and annotate interactable parts for all bad predictions (the definitions of what classifies a result as perfect/fair/bad were provided to the users beforehand, as also explained in the beginning of this section).

We use labelme[28] as the labeling tool. The average times taken by humans for different tasks in our AL model are as follows: time to identify whether the prediction is perfect, fair or bad $\tau_{ident} = 2.4s$, time to click the corresponding selection button in our interface $\tau_{click} = 0.6s$, and average per-annotation labeling time $\tau_{anno} = 14.8s$. We also attach a video in the supplementary material showing the interface of our AL setup for sample selection and annotation.

Table 8: Different data and efficiency statistics over each iteration of the active learning process on the *enhancement set* using Mask2Former.

Iter.	Train	Test	Perfect	Bad	Time (hr)
0	50	500	-	-	-
1	256	294	176	30 / 106	0.997
2	339	211	58	25 / 88	0.693
3	398	152	32	27 / 95	0.630
4	437	113	27	12 / 42	0.344
5	471	79	15	19 / 68	0.409
6	505	45	14	20 / 71	0.384
7	550	-	20	25 / 90	0.425
Total:				158 / 560	3.882

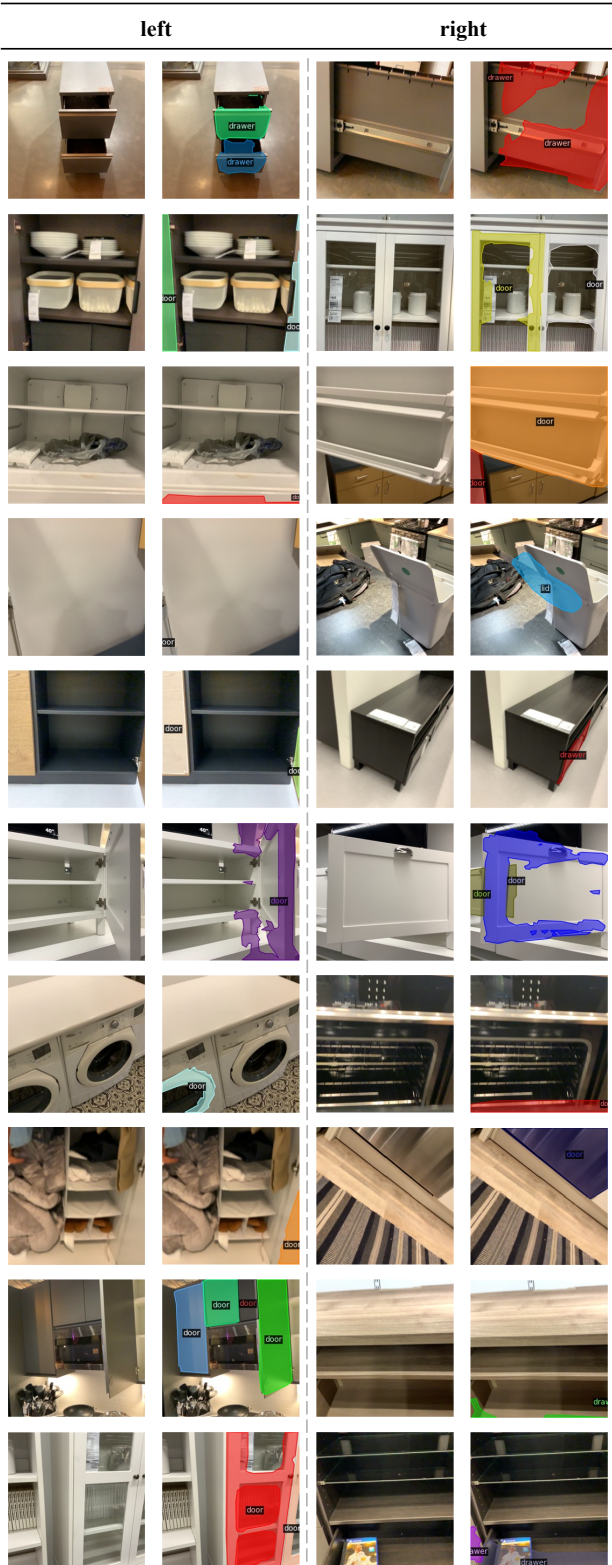
Table 9: Different data and efficiency statistics over each iteration of the active learning process on the *enhancement set* using OPDRCNN-C.

Iter.	Train	Test	Perfect	Bad	Time (hr)
0	50	500	-	-	-
1	129	421	17	62 / 211	1.435
2	207	343	36	42 / 143	1.064
3	293	257	46	40 / 145	0.985
4	384	166	52	39 / 128	0.819
5	450	100	32	34 / 108	0.634
6	512	38	35	27 / 95	0.507
7	550	-	21	17 / 57	0.280
Total:				261 / 887	5.724

Table 10: Different data and efficiency statistics over each iteration of the active learning process on the 2000 test images using our method.

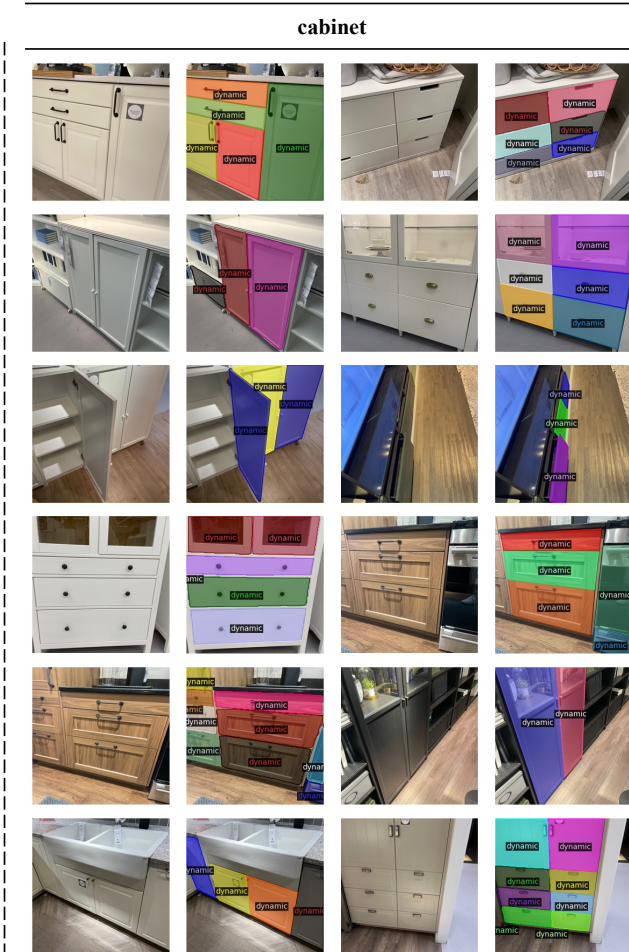
Iter.	Train	Test	Perfect	Bad	Time (hr)
0	50	2000	-	-	-
1	1761	739	1143	118 / 392	3.856
2	2255	245	392	102 / 341	2.242
3	2399	101	102	42 / 156	0.922
4	2500	-	74	27 / 94	0.504
Total:				289 / 983	7.524

OPDReal



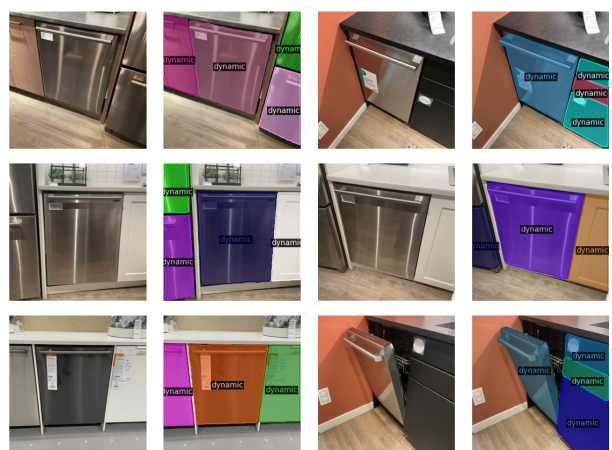
(a)

ours



(b)

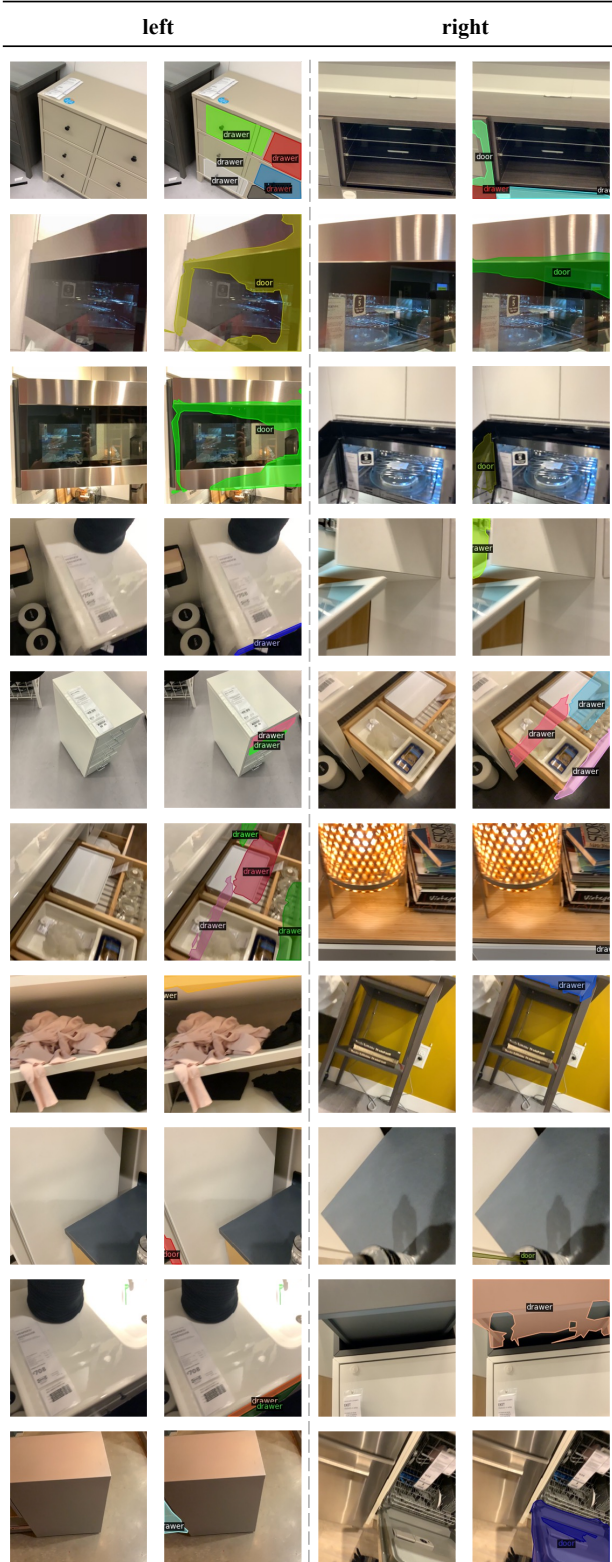
dishwasher



(c)

Figure 5: Visualizations of dataset annotations of OPDReal and ours. (No AL) (Part 1)

OPDReal



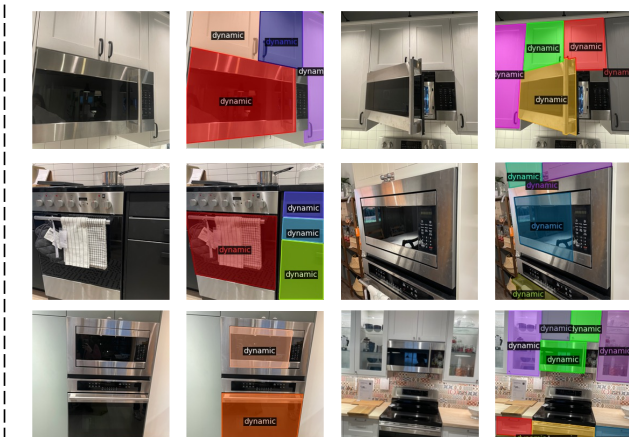
(a)

ours



(b)

microwave & oven



(c)

washing machine



(d)

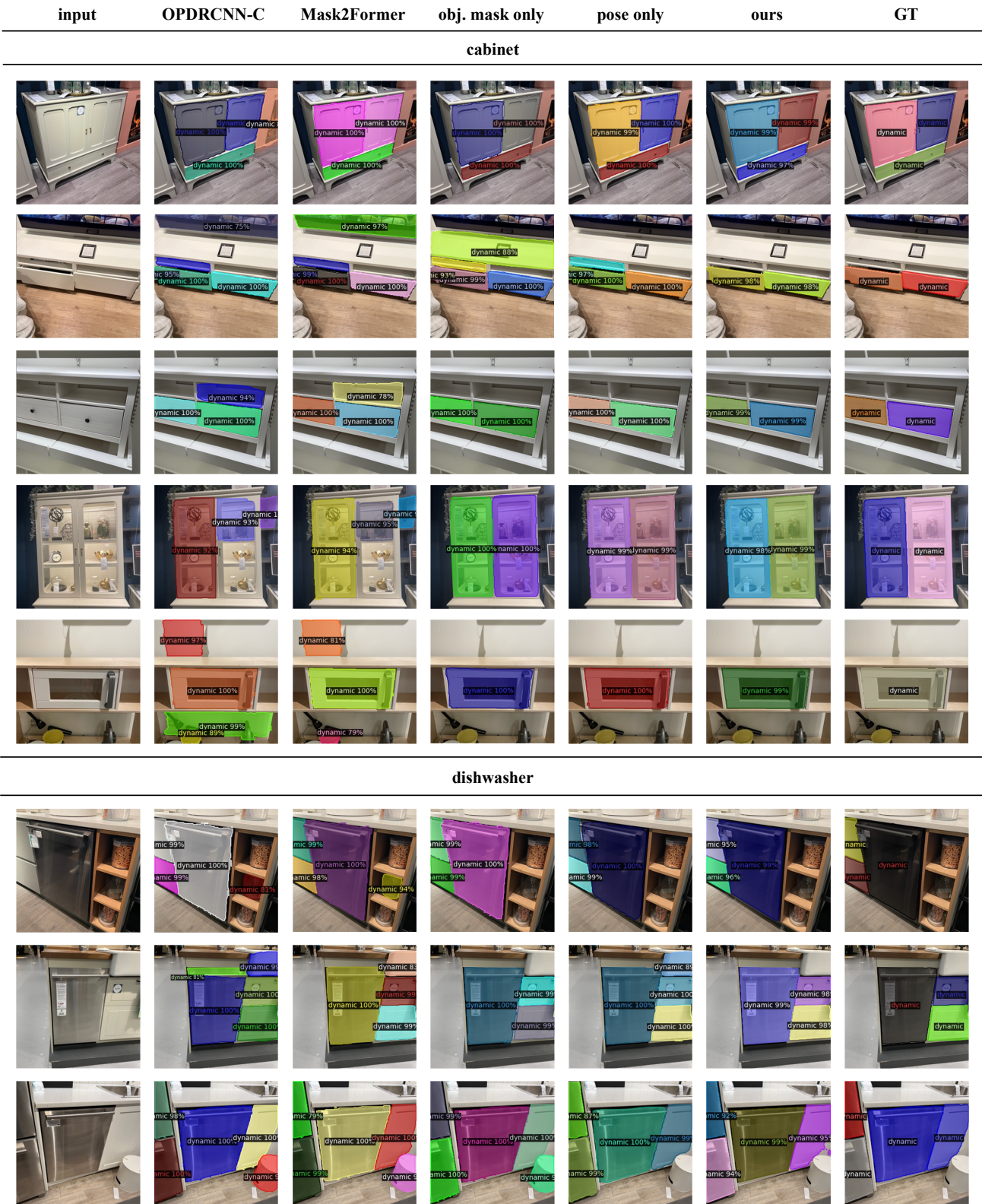


Figure 7: Qualitative results of different methods on our test set (No AL) (cabinet and dishwasher).

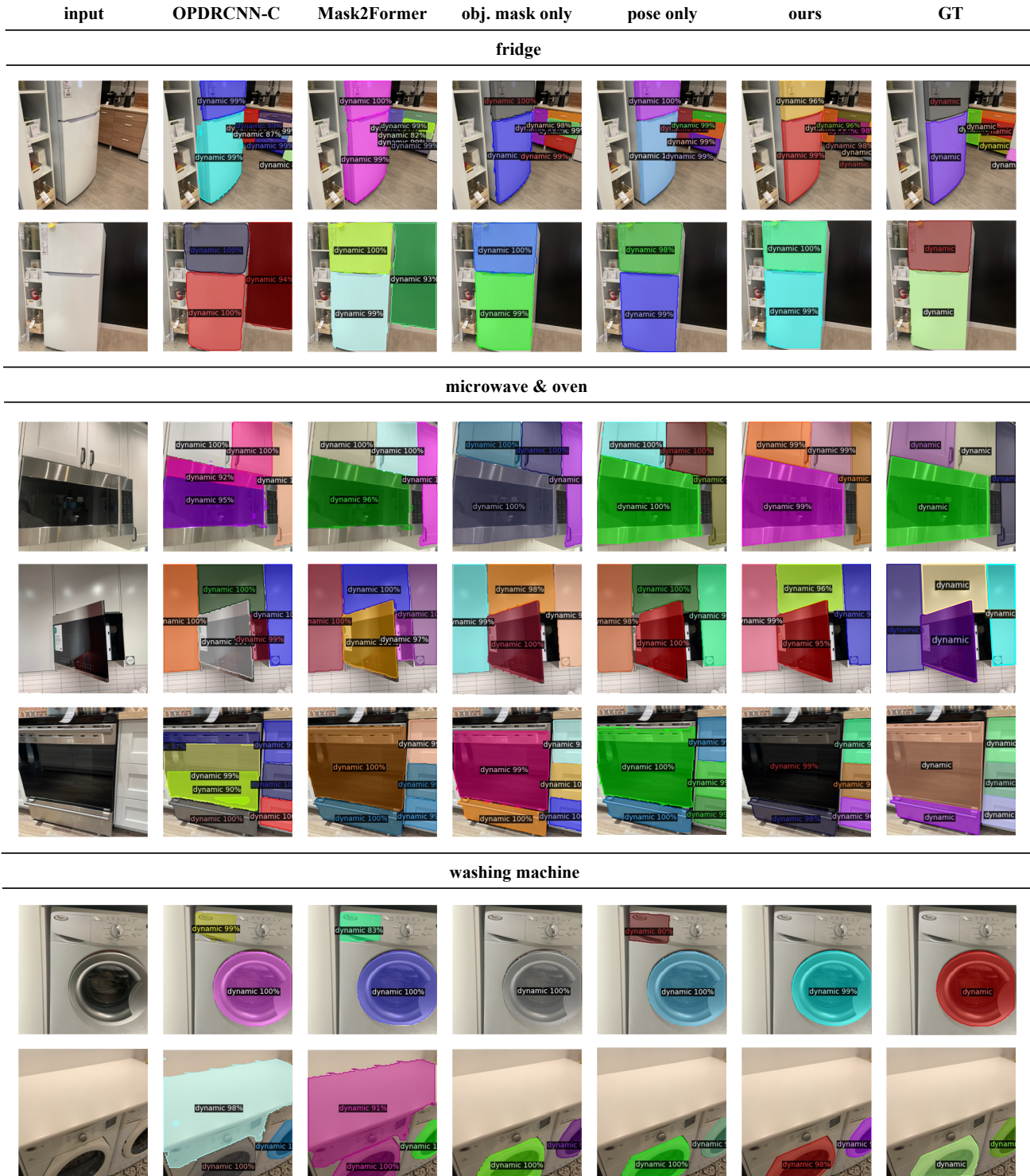


Figure 8: Qualitative results of different methods on our test set (No AL) (fridge, microwave & oven and washing machine).

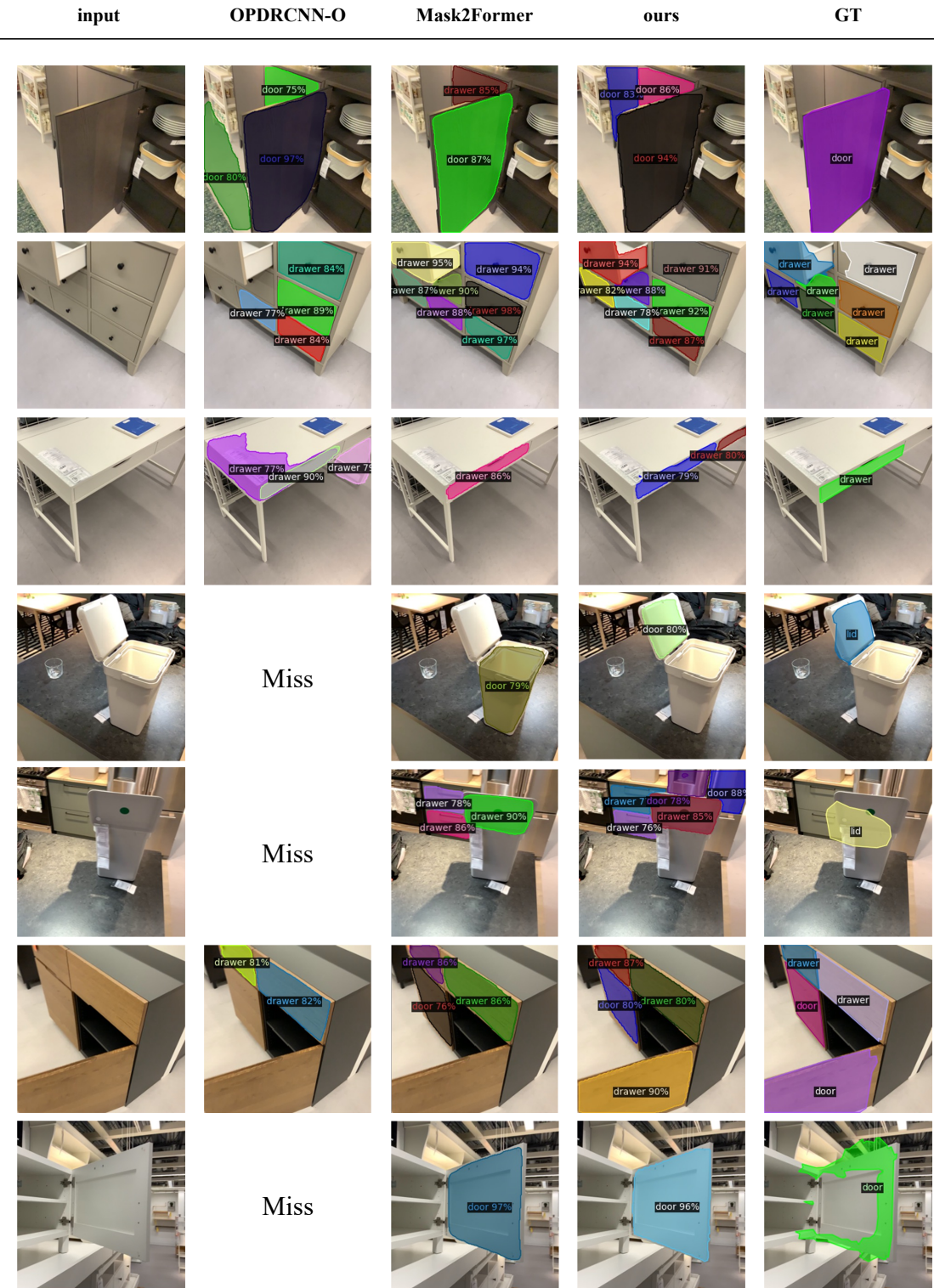


Figure 9: Qualitative results of different methods on OPDReal test set (No AL) (Part 1).

